Combined GW and dynamical mean field theory: Dynamical screening effects in transition metal oxides

Jan M. Tomczak,[1] Michele Casula,[2] Takashi Miyake,[3,4] Ferdi Aryasetiawan,[5] and Silke Biermann[6,4]

[1]*Department of Physics and Astronomy, Rutgers University, Piscataway, New Jersey 08854, USA*
[2]*CNRS and Institut de Minéralogie et de Physique des Milieux condensés, Université Pierre et Marie Curie, case 115, 4 place Jussieu, 75252, Paris cedex 05, France*
[3]*Nanosystem Research Institute (NRI) RICS, AIST, Tsukuba, Ibaraki 305-8568, Japan*
[4]*Japan Science and Technology Agency, CREST, Kawaguchi 332-0012, Japan*
[5]*Department of Physics, Mathematical Physics, Lund University, Sölvegatan 14A, 22362 Lund, Sweden*
[6]*Centre de Physique Théorique, Ecole Polytechnique, CNRS UMR 7644, 91128 Palaiseau Cedex, France*

We present the first dynamical implementation of the combined GW and dynamical mean field scheme ("GW+DMFT") for first principles calculations of the electronic properties of correlated materials. The application to the ternary transition metal oxide $SrVO_3$ demonstrates that this schemes inherits the virtues of its two parent theories: a good description of the local low energy correlation physics encoded in a renormalized quasi-particle band structure, spectral weight transfer to Hubbard bands, and the physics of screening driven by long-range Coulomb interactions. Our data is in good agreement with available photoemission and inverse photoemission spectra; our analysis leads to a reinterpretation of the commonly accepted "three-peak structure" as originating from orbital effects rather than from the electron addition peak within the t_{2g} manifold.

PACS numbers:

Describing electronic excitations of materials with strong electronic Coulomb interactions remains one of the challenges of modern condensed matter theory [1]. Photoemission satellite features, quasi-particle mass renormalizations or – in the strong coupling limit – the localization of electrons are phenomena well beyond band theory. Within effective low-energy models, such as the Hubbard or Anderson lattice model, insight has been gained into the low-energy physics of correlated materials on a qualitative level. However, when relating this knowledge to specific materials, attempting a *quantitative* description, several challenges persist: The first one is a question of energy scales: in fact, much of the physics of interest in correlated materials takes place on the scale of several eV, well beyond what is captured within a low-energy description. Optical properties of transition metal oxides, to cite a specific example, are determined by the onset of optical transitions involving ligand states already at scales of only a few eV. A second issue is the determination of the model parameters, e.g., the effective low-energy hopping parameters and Coulomb interactions, in particular the local "Hubbard U". These two issues are in fact intimately related, since high energy screening processes renormalize these parameters, and an appropriately downfolded low-energy model should take this into account [2–7].

In this Letter, we present the first *dynamical* implementation of a combined GW and dynamical mean field ("GW+DMFT") scheme that addresses the above issues, by treating explicitly both, dynamical Coulomb interactions on the "correlated" manifold of orbitals, and corrections to the band structure of degrees of freedom that live on higher energy scales. The application to a well-studied correlated metal, $SrVO_3$, shows some expected features: a renormalization of the quasiparticle band structure, the formation of a lower Hubbard band and the correction of the position of the oxygen p-states. It also leads to less expected features, namely the absence of a clearly distinguishable upper Hubbard band in the total spectral function along with a reinterpretation of the feature seen at about 2.7 eV in inverse photoemission that we associate with the e_g states. This attribution is in agreement with cluster model calculations [8] and allows to resolve apparent contradictions between cluster and dynamical mean field methods for this compound. In the orbital-resolved spectral function we furthermore predict additional satellite features induced by the frequency-dependence of the effective Coulomb interaction.

The combined GW+DMFT scheme was proposed a few years ago, in order to avoid the ad hoc nature of the Hubbard parameter and the double counting inherent to conventional combinations of dynamical mean field theory with density functional theory in the local density approximation (so-called "LDA+DMFT" schemes[9, 10]). The starting point is Hedin's GW approximation (GWA)[11], in which the self-energy of a quantum many-body system is obtained as a product of the Green's function G and the screened Coulomb interaction $W = \epsilon^{-1}V$. The dielectric function ϵ, which screens the bare Coulomb potential V, is –within a pure GW scheme– obtained from the random phase approximation. The GW+DMFT scheme, as proposed in [12], combines the first principles description of screening inherent in GW methods with the non-perturbative nature of DMFT, where local quantities such as the local Green's function are calculated to all orders in the interaction

from an effective reference system ("impurity model"). In DMFT, one imposes a self-consistency condition for the one-particle Green's function, namely, that its on–site projection equals the impurity Green's function. In GW+DMFT, the self-consistency requirement is generalized to encompass two-particle quantities as well, namely, the local projection of the screened interaction is required to equal the impurity screened interaction. This in principle promotes the Hubbard U from an adjustable parameter in DMFT techniques to a self-consistent auxiliary function that incorporates long-range screening effects in an *ab initio* fashion. Moreover, the theory provides momentum dependence to quantities (such as the self-energy) that are local within pure DMFT. Despite these conceptually attractive features, however, no dynamical implementation, even at the non-selfconsistent level has been achieved so far (see however the static implementation in [12], as well as model studies of a one-band extended Hubbard model in [13, 14]).

From a formal point of view, the GW+DMFT method, as introduced in Ref. [12], corresponds to a specific approximation to the correlation part of the free energy of a solid, expressed as a functional of the Green's function G and the screened Coulomb interaction W : the non-local part is taken to be the first order term in W, while the local part is calculated from an impurity model as in (extended) dynamical mean field theory. This leads to a set of self-consistent equations for G, W, the self-energy Σ and the polarization P [15, 16]. Specifically, the self-energy is obtained as $\Sigma = \Sigma_{local} + \Sigma^{GW}_{non-local}$, where the local part Σ_{local} is derived from the impurity model[56]. In practice, however, s- or p-orbitals are rather delocalized. Here, we therefore propose a practical scheme, in which only the local part of the self-energy of the "correlated" orbitals is obtained from an impurity reference, and all other local and non-local components are approximated by their first order expressions in W. Green's functions and self-energies are expressed as matrices in a basis of atom-centered Wannier functions[57]. For practical reasons, we avoid the costly GW self-consistency cycle, and in particular the update of the dynamical interaction $U(\omega)$: Instead, we calculate $U(\omega)$ from the constrained random phase approximation (cRPA) [2, 17, 18] and keep it fixed when iterating the local one-particle quantities to self-consistency.[58]

Our target material, $SrVO_3$, crystallizes in the cubic perovskite structure: the V^{4+} ions are surrounded by oxygen octahedra, occupying the sites of a simple cubic lattice. The Sr^{2+} cation sits in the center of the cubes. The electron count leaves a single d electron in the V-d states, which is largely responsible for the electronic properties of the compound. The octahedral crystal field splits the V-d states into a lower-lying threefold degenerate t_{2g} manifold, thus filled with one electron per V, and an empty e_g doublet. The compound exhibits metallic resistivity with a Fermi liquid T^2 behavior up to room temperature [19] and temperature-independent Pauli paramagnetism without any sign of magnetic ordering [20]. Hall data and NMR measurements [19, 21] as well as angle-resolved photoemission spectra [22] that find the Fermi surface of $SrVO_3$ as cylindrical Fermi sheets, in agreement with theory, confirm the picture of a normal Fermi liquid.

These properties make $SrVO_3$ an ideal model material for studying the effects of electronic Coulomb interactions [8, 23–35]. Recent works include, e.g., studies of surface effects [36], kink structures in the momentum-resolved spectral function [37–39], or non-local correlation effects [40, 41] in relation to laser ARPES [42] which finds a "dip" at the Fermi level or a maximum of the quasiparticle peak slightly below (at around -0.2 eV). The experimentally observed quasiparticle weight is about 0.5-0.6 [23, 43–49], with the remaining spectral weight being carried by a photoemission (PES) (Hubbard-)satellite at around -1.6 eV [47, 50]. Inverse photoemission (BIS) has located the electron addition $d^1 \rightarrow d^2$ peak at an energy of about 2.7 eV [50].

Figure 1a summarizes the LDA electronic structure: the O-p states disperse between -2 and -7 eV, separated from the t_{2g} states whose bandwidth extends from -1 eV to 1.5 eV. While the t_{2g} and e_g bands are well separated at every given k-point, the partial density of states (DOS) slightly overlap, and the e_g states display a pronounced peak at 2.3 eV. Finally, peaks stemming from the Sr-d states are located at 6.1 eV and 7.1 eV. We have superimposed to the LDA DOS the experimental PES and BIS curves taken from [47, 50]. The comparison reveals the main effects of electronic correlations in this material: as expected on quite general grounds, LDA locates the filled O-p states at too high and the empty Sr-d manifold at too low energies. The t_{2g} manifold undergoes a strong quasi-particle renormalization with a concomitant shift of spectral weight to the lower Hubbard band, both of which are effects beyond the one-particle picture.

Applying the GW approximation (see the spectral function in Fig. 1b) increases the O-p to Sr-d distance, placing both manifolds at energies nearly in agreement with experiment[59]. Most interestingly, however, a peak at 2.6 eV emerges from the d-manifold, which we find to be of e_g character. Indeed, the GW approximation enhances the crystal field splitting and places the maximum of the e_g spectral weight at the location of the experimentally observed $d^1 \rightarrow d^2$ addition peak.

Also displayed is the partial t_{2g} contribution. Two interesting points are seen : the quasi-particle width is narrowed from the LDA value by about 0.5 eV and satellite structures appear below and above the Fermi level at ± 3 eV, $+5$eV as well as at around 15eV. Within the (non-self-consistent) GW approximation, the self-energy

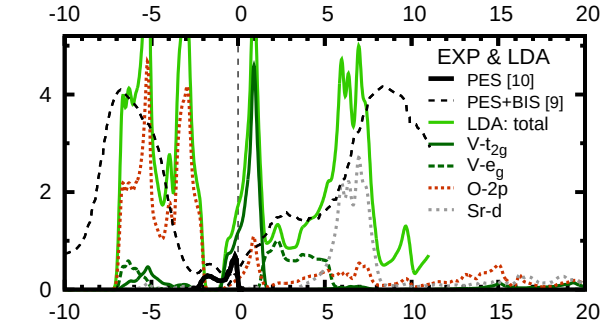

(a)

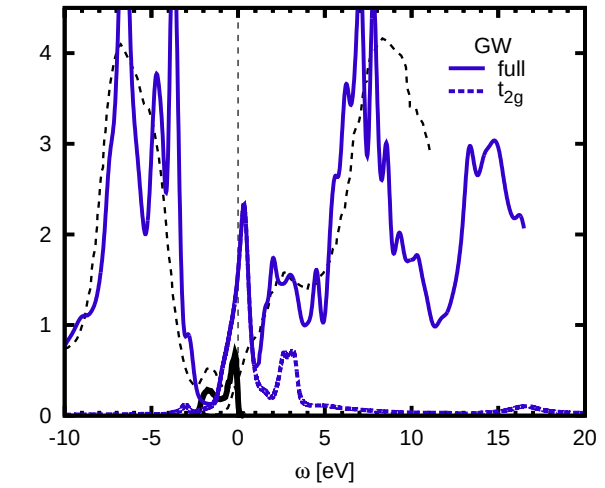

(b)

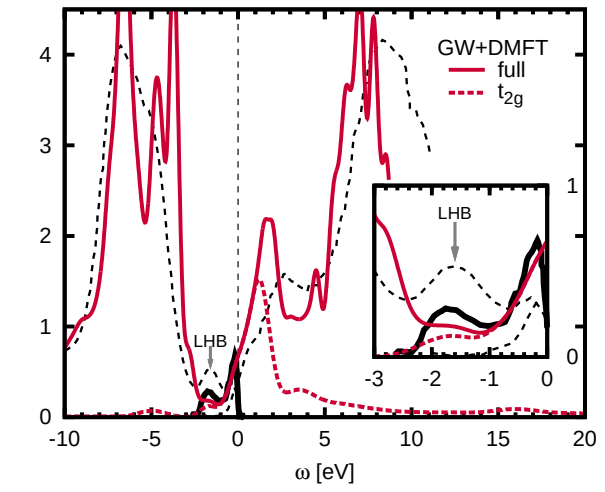

(c)

FIG. 1: (a) Orbital-resolved LDA density of states, in comparison to experimental spectra from photoemission (PES)[47, 50] and inverse photoemission (BIS)[47]. The latter are reproduced also in panels (b-c). (b) Spectral function from GW (full orbital and t_{2g} only) in comparison to experiments. (c) Spectral function from GW+DMFT (full orbital and t_{2g} only) in comparison to experiments. The inset shows a low energy zoom. In the GW+DMFT spectrum, LHB denotes the lower Hubbard band. See text for details.

is related to ImW as follows :

$$\mathrm{Im}\Sigma_{GW}(r,r';\omega) \;=\; \sum_{kn} \psi_{kn}(r)\mathrm{Im}W(r',r;\varepsilon_{kn}-\omega)\psi^{*}_{kn}(r')$$

Thus, a feature at ω_0 in ImW causes a satellite feature at an energy ω_0 below or above the quasiparticle peak at ε_{kn}. In Fig. 2 we display the on-site t_{2g} intra–orbital element W_{t2g} of the fully screened interaction in the Wannier basis. Three notable features are clearly discernible: There is the usual high-energy electron-gas-like plasmon excitation at around 15 eV and, more remarkably, there is a strong excitation between 2–3 eV, as well as a shoulder at ∼4.5eV. Evidently, these energy positions directly correlate with the spectral features discussed above. It is important to note that the lowest feature in W_{t2g} mainly arises from a collective excitation within the t_{2g} bands. This can be understood by comparison with the Hubbard interaction $U(\omega)$ of the low energy t_{2g} system, as calculated within the constrained RPA. In $U(\omega)$ the structure at 2∼3 eV is absent, due to the elimination of the polarization within the t_{2g} bands. The shoulder at around 4.5eV, however, partly persists, as its excitations also involve O-2p states; we will come back to this point below.

Solving the GW+DMFT equations, even without the self-consistency cycle at the GW level, that is, for fixed $\Sigma^{non-local}_{GW}$ and $U(\omega)$, is a hard task. We use the scheme recently introduced in Ref. [4]: the Green's function of the dynamical impurity model is obtained from a factorization ansatz $G(\tau) = G_{stat}(\tau)B(\tau)$ where G_{stat} is the Green's function of a static impurity model with constant U=$U(\omega$=0)[60], and the second factor $B(\tau) = G(\tau)/G_{stat}(\tau)$ is approximated by its value for vanishing bath hybridization Δ[4] :

$$B(\tau) = \exp\left(-\int_0^\infty \frac{d\omega}{\pi}\frac{\mathrm{Im}U(\omega)}{\omega^2}\left[K_\tau(\omega)-K_0(\omega)\right]\right) \quad (1)$$

with $K_\tau(\omega) = \frac{\exp(-\tau\omega)+\exp(-(\beta-\tau)\omega)}{1-\exp(-\beta\omega)}$. In the regime that we are interested in, namely when the plasma frequency is several times the bandwidth, this is an excellent approximation[4].

Finally, we present our GW+DMFT results for the spectrum of $SrVO_3$ at inverse temperature β=10eV^{-1} : Fig. 1(c) displays the local projection, while Fig. 3 shows momentum dependent t_{2g} spectra in comparison with ARPES measurements[39, 48]. The low-energy part of the spectrum is dominated by the t_{2g} contribution, which, here, is profoundly modified with respect to pure GW results. A renormalized quasi-particle band disperses around the Fermi level : At the Γ point the peak is located at about -0.5 eV – a strong renormalization of the corresponding Kohn-Sham state which, at this momentum, has an energy of -1 eV. At the X-point, the t_{2g} bands are no longer degenerate, and surprisingly weakly renormalized xy/xz states are observed at 0.9 eV, while the yz band is located at nearly the same energy as at

the Γ point, in agreement with ARPES. At binding energies of 1.6 eV, ARPES witnesses a weakly dispersive Hubbard band, whose intensity varies significantly as a function of momentum [48]. In the GW+DMFT spectral function the Hubbard band – absent in GW – is correctly observed at about -1.6 eV, and its k-dependent intensity variation (see Fig. 3) is indeed quite strong. Previous LDA+DMFT calculations placed the lower Hubbard band at larger negative energies (see e.g. [27]). This is owing to the fact that when using a static Hubbard interaction, a value of 4–6 eV, that is larger than the zero frequency limit of the *ab intio* $U(\omega{=}0){=}3.6$eV[18], is needed to account for the observed transfers of spectral weight. LDA+$U(\omega)$+DMFT calculations taking not only the *ab initio* value of the static component of U but also its full frequency dependence into account indeed reproduce the position of the lower Hubbard band quite well [4, 51]. Analogously, in GW+DMFT, the additional transfers from the dynamical screening [4, 6, 52], yield a good description of the Hubbard band and the spectral weight reduction at the same time.

At positive energies non-local self-energy effects are larger. Interestingly, our total spectral function, Fig.1(c), does not display a clearly separated Hubbard band. The reason is visible from the k-resolved spectra: the upper Hubbard band is located at around 2 eV, as expected from the location of the lower Hubbard band and the fact that their separation is roughly given by the zero-frequency value of U. The peak around 2.7 eV that appears in the inverse photoemission spectrum [50] – commonly interpreted as the upper Hubbard band of t_{2g} character in the DMFT literature – arises in fact from e_g states located in this energy range. The non-local self-energy effects lead, in the unoccupied part of the spectrum, to overlapping features from different k-points and an overall smearing of the total spectral function.

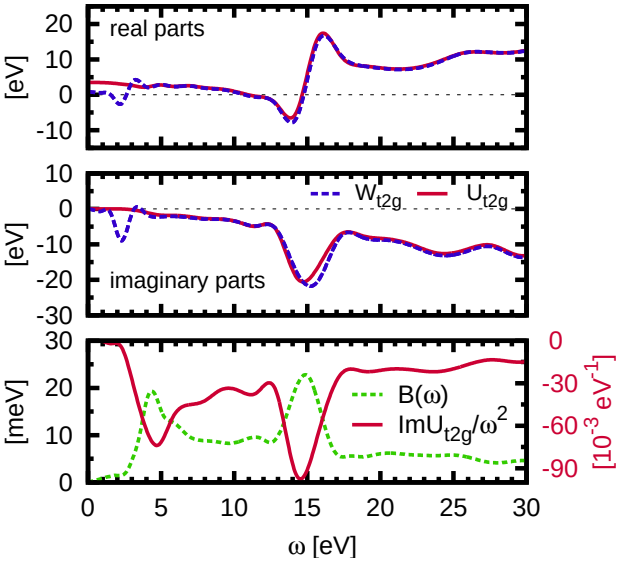

FIG. 2: (Partially) screened Coulomb interactions for $SrVO_3$: ReU, ReW (top panel), ImU, ImW (middle). ImU/ω^2 and plasmon spectral function $B(\omega)$ (bottom).

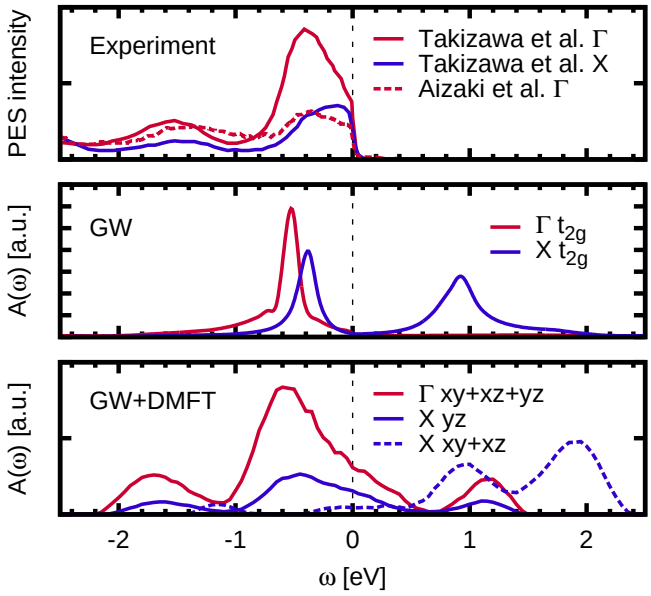

FIG. 3: Momentum-resolved t_{2g} spectral functions from GW and GW+DMFT, compared to experimental angle resolved photoemission spectra of Refs. [39] and [48]. The GW spectra are calculated at zero temperature.

Akin to the correspondence between ImW and the GW spectrum, our approach to solve the GW+DMFT equations allows for a transparent physical interpretation of the arising spectral properties. Indeed the spectral representation of the bosonic renormalization factor $B(\tau)$ of Eq. 1 (displayed in the lower panel of Fig. 2) is directly related to the density of screening modes Im$U(\omega)/\omega^2$ [4]. In this way, we can trace back the GW+DMFT satellite at -4.5 eV to the onset of p-t_{2g} excitations, discussed above for W and U. On the other hand, since the feature below 3 eV in W is absent in U and B, at least the local self-energy contribution to the corresponding peak within GW does not survive in GW+DMFT. The strong peak at 15 eV is the well-known plasma excitation, seen e.g. in electron energy loss spectra of $SrTiO_3$[53].

In conclusion, we have presented the first dynamical implementation of a combined GW and dynamical mean field scheme. Quite generally, materials with a "double LDA failure"– an inappropriate description of correlated states, and deficiencies of LDA for the more itinerant states, such as an underestimated "*pd*-gap" – can be treated within our scheme. Application to a well-studied benchmark material, $SrVO_3$, confirms the ability of the approach to describe simultaneously Hubbard bands, higher energy satellite structures and corrected energy gaps, in an *ab initio* fashion. In the unoccupied part of the one-particle spectral function, we attribute

a strong peak evidenced in BIS spectra to the electron addition process into the e_g states, in agreement with cluster studies [8]. We further predict the existence of a satellite feature at -4.5 eV, that may seem difficult to resolve experimentally because of its overlap with oxygen p-states. Nevertheless we would expect that a systematic PES study as a function of photon energy, due to the dependence of the cross section on orbital characters, could possibly resolve this feature. In fact, structures of similar origin may already have been observed in other materials, such as e.g. in VO_2 [54] and iron pnictides [5].

We thank A. Fujimori for useful discussions and for making the data of Ref. [39] available to us prior to publication. This work was supported by the French ANR under project SURMOTT, and a grant of supercomputing time at IDRIS/GENCI under project number 1393.

[1] M. Imada, A. Fujimori, and Y. Tokura, Rev. Mod. Phys. **70**, 1039 (1998).
[2] F. Aryasetiawan, M. Imada, A. Georges, G. Kotliar, S. Biermann, and A. I. Lichtenstein, Phys. Rev. B **70**, 195104 (2004).
[3] Y. Imai, I. Solovyev, and M. Imada, Phys. Rev. Lett. **95**, 176405 (2005).
[4] M. Casula, A. Rubtsov, and S. Biermann, Phys. Rev. B **85**, 035115 (2012).
[5] P. Werner, M. Casula, T. Miyake, F. Aryasetiawan, A. J. Millis, and S. Biermann, Nat. Phys. **8**, 331 (2012).
[6] M. Casula, P. Werner, L. Vaugier, F. Aryasetiawan, T. Miyake, A. J. Millis, and S. Biermann, Phys. Rev. Lett. **109**, 126408 (2012).
[7] F. Aryasetiawan, J. M. Tomczak, T. Miyake, and R. Sakuma, Phys. Rev. Lett. **102**, 176402 (2009).
[8] R. J. O. Mossanek, M. Abbate, T. Yoshida, A. Fujimori, Y. Yoshida, N. Shirakawa, H. Eisaki, S. Kohno, P. T. Fonseca, and F. C. Vicentin, Phys. Rev. B **79**, 033104 (2009).
[9] A. I. Lichtenstein and M. I. Katsnelson, Phys. Rev. B **57**, 6884 (1998).
[10] V. I. Anisimov, A. I. Poteryaev, M. A. Korotin, A. O. Anokhin, and G. Kotliar, J. Phys.: Cond. Matter **9**, 7359 (1997).
[11] L. Hedin, Phys. Rev. **139**, A796 (1965).
[12] S. Biermann, F. Aryasetiawan, and A. Georges, Phys. Rev. Lett. **90**, 086402 (2003).
[13] P. Sun and G. Kotliar, Phys. Rev. Lett. **92**, 196402 (2004).
[14] T. Ayral, P. Werner, and S. Biermann, Phys. Rev. Lett. **109**, 226401 (2012).
[15] S. Biermann, F. Aryasetiawan, and A. Georges, Proceedings of the NATO Advanced Research Workshop on "Physics of Spin in Solids: Materials, Methods, and Applications" in Baku, Azerbaijan, Oct. 2003. NATO Science Series II, Kluwer Academic Publishers B.V (2004).
[16] F. Aryasetiawan, S. Biermann, and A. Georges, Proceedings of the conference "Coincidence Studies of Surfaces, Thin Films and Nanostructures", Ringberg castle, Sept. 2003 (2004).
[17] F. Aryasetiawan, K. Karlsson, O. Jepsen, and U. Schönberger, Phys. Rev. B **74**, 125106 (2006).
[18] T. Miyake and F. Aryasetiawan, Phys. Rev. B **77**, 085122 (2008).
[19] M. Onoda, H. Ohta, and H. Nagasawa, Solid State Communications **79**, 281 (1991), ISSN 0038-1098.
[20] I. Inoue, H. Makino, I. Hase, M. Ishikawa, N. Hussey, and M. Rozenberg, Physica B: Condensed Matter **237238**, 61 (1997), ISSN 0921-4526, Proceedings of the Yamada Conference XLV, the International Conference on the Physics of Transition Metals.
[21] H. Eisaki (PhD thesis, Tokyo University, 1991).
[22] T. Yoshida, K. Tanaka, H. Yagi, A. Ino, H. Eisaki, A. Fujimori, and Z.-X. Shen, Phys. Rev. Lett. **95**, 146404 (2005).
[23] A. Fujimori, I. Hase, H. Namatame, Y. Fujishima, Y. Tokura, H. Eisaki, S. Uchida, K. Takegahara, and F. M. F. de Groot, Phys. Rev. Lett. **69**, 1796 (1992).
[24] R. J. O. Mossanek, M. Abbate, and A. Fujimori, Phys. Rev. B **74**, 155127 (2006).
[25] R. J. O. Mossanek, M. Abbate, T. Yoshida, A. Fujimori, Y. Yoshida, N. Shirakawa, H. Eisaki, S. Kohno, and F. C. Vicentin, Phys. Rev. B **78**, 075103 (2008).
[26] H. Wadati, A. Chikamatsu, M. Takizawa, H. Kumigashira, T. Yoshida, T. Mizokawa, A. Fujimori, M. Oshima, and N. Hamada, J. Phys. Soc. Jpn. **78**, 094709 (2009).
[27] E. Pavarini, S. Biermann, A. Poteryaev, A. I. Lichtenstein, A. Georges, and O. K. Andersen, Phys. Rev. Lett. **92**, 176403 (2004).
[28] I. A. Nekrasov, G. Keller, D. E. Kondakov, A. V. Kozhevnikov, T. Pruschke, K. Held, D. Vollhardt, and V. I. Anisimov, Phys. Rev. B **72**, 155106 (2005).
[29] E. Pavarini, A. Yamasaki, J. Nuss, and O. K. Andersen, New Journal of Physics **7**, 188 (2005).
[30] V. I. Anisimov, D. E. Kondakov, A. V. Kozhevnikov, I. A. Nekrasov, Z. V. Pchelkina, J. W. Allen, S.-K. Mo, H.-D. Kim, P. Metcalf, S. Suga, et al., Phys. Rev. B **71**, 125119 (2005).
[31] F. Lechermann, A. Georges, A. Poteryaev, S. Biermann, M. Posternak, A. Yamasaki, and O. K. Andersen, Phys. Rev. B **74**, 125120 (2006).
[32] G. Trimarchi, I. Leonov, N. Binggeli, D. Korotin, and V. I. Anisimov, Journal of Physics: Condensed Matter **20**, 135227 (2008).
[33] M. Aichhorn, L. Pourovskii, V. Vildosola, M. Ferrero, O. Parcollet, T. Miyake, A. Georges, and S. Biermann, Phys. Rev. B **80**, 085101 (2009).
[34] M. Karolak, T. O. Wehling, F. Lechermann, and A. I. Lichtenstein, Journal of Physics: Condensed Matter **23**, 085601 (2011).
[35] B. Amadon, F. Lechermann, A. Georges, F. Jollet, T. O. Wehling, and A. I. Lichtenstein, Phys. Rev. B **77**, 205112 (2008).
[36] A. Liebsch, Phys. Rev. Lett. **90**, 096401 (2003).
[37] I. A. Nekrasov, K. Held, G. Keller, D. E. Kondakov, T. Pruschke, M. Kollar, O. K. Andersen, V. I. Anisimov, and D. Vollhardt, Phys. Rev. B **73**, 155112 (2006).
[38] K. Byczuk, M. Kollar, K. Held, Y. F. Yang, I. A. Nekrasov, T. Pruschke, and D. Vollhardt, Nat Phys **3**, 168 (2007).
[39] S. Aizaki, T. Yoshida, K. Yoshimatsu, M. Takizawa, M. Minohara, S. Ideta, A. Fujimori, K. Gupta, P. Mahadevan, K. Horiba, et al., Phys. Rev. Lett. **109**, 056401

(2012).
[40] Y. Z. Zhang and M. Imada, Phys. Rev. B **76**, 045108 (2007).
[41] H. Lee, K. Foyevtsova, J. Ferber, M. Aichhorn, H. O. Jeschke, and R. Valentí, Phys. Rev. B **85**, 165103 (2012).
[42] R. Eguchi, T. Kiss, S. Tsuda, T. Shimojima, T. Mizokami, T. Yokoya, A. Chainani, S. Shin, I. H. Inoue, T. Togashi, et al., Phys. Rev. Lett. **96**, 076402 (2006).
[43] I. Inoue, *Electronic States of Correlated Transition Metal Oxides: Ca1-xSrxVO3 and Sr2RuO4* (PhD thesis, Tokyo University, 1998).
[44] I. H. Inoue, O. Goto, H. Makino, N. E. Hussey, and M. Ishikawa, Phys. Rev. B **58**, 4372 (1998).
[45] K. Maiti, D. D. Sarma, M. J. Rozenberg, I. H. Inoue, H. Makino, O. Goto, M. Pedio, and R. Cimino, EPL (Europhysics Letters) **55**, 246 (2001).
[46] K. Maiti, U. Manju, S. Ray, P. Mahadevan, I. H. Inoue, C. Carbone, and D. D. Sarma, Phys. Rev. B **73**, 052508 (2006).
[47] A. Sekiyama, H. Fujiwara, S. Imada, S. Suga, H. Eisaki, S. I. Uchida, K. Takegahara, H. Harima, Y. Saitoh, I. A. Nekrasov, et al., Phys. Rev. Lett. **93**, 156402 (2004).
[48] M. Takizawa, M. Minohara, H. Kumigashira, D. Toyota, M. Oshima, H. Wadati, T. Yoshida, A. Fujimori, M. Lippmaa, M. Kawasaki, et al., Phys. Rev. B **80**, 235104 (2009).
[49] T. Yoshida, M. Hashimoto, T. Takizawa, A. Fujimori, M. Kubota, K. Ono, and H. Eisaki, Phys. Rev. B **82**, 085119 (2010).
[50] K. Morikawa, T. Mizokawa, K. Kobayashi, A. Fujimori, H. Eisaki, S. Uchida, F. Iga, and Y. Nishihara, Phys. Rev. B **52**, 13711 (1995).
[51] L. Huang and Y. Wang, ArXiv e-prints (2012), 1205.6965.
[52] P. Werner and A. J. Millis, Phys. Rev. Lett. **104**, 146401 (2010).
[53] S. Kohiki, M. Arai, H. Yoshikawa, S. Fukushima, M. Oku, and Y. Waseda, Phys. Rev. B **62**, 7964 (2000).
[54] R. Eguchi, M. Taguchi, M. Matsunami, K. Horiba, K. Yamamoto, Y. Ishida, A. Chainani, Y. Takata, M. Yabashi, D. Miwa, et al., Phys. Rev. B **78**, 075115 (2008).
[55] N. Marzari and D. Vanderbilt, Phys. Rev. B **56**, 12847 (1997).
[56] The notion of locality refers to the use of a specific basis set of atom-centered orbitals, such as muffin-tin orbitals, or atom-centered Wannier functions.
[57] We choose a maximally localized Wannier basis[18, 55] constructed separately for the correlated (t_{2g}) and uncorrelated subspaces, such that the one-particle Hamiltonian is blockdiagonal. Then, off-blockdiagonal self-energy elements are small and neglected in the following. Also, the local part of the free energy functional then separates into correlated and uncorrelated subspace contributions. Our approach consists in calculating only the former from the impurity model, and the latter to first order in W.
[58] The GW calculation was performed for a 4x4x4 k-point mesh, the t_{2g} part of which was Wannier interpolated onto a 27^3 mesh for the GW+DMFT self-consistency.
[59] The persisting slight underestimation is expected : (a) the polarization (determining W) is derived from the bare t_{2g} bands, whose character is largely too itinerant in LDA, and (b) vertex corrections are neglected.
[60] For the Hund's rule coupling the static cRPA value $J =$ 0.5eV is used.